J Mater Sci (2021) 56:10092–10107

Metals & corrosion

Uncovering the influence of Cu on the thickening and strength of the $\delta'/\theta'/\delta'$ nano-composite precipitate in Al–Cu–Li alloys

Shuo Wang[1], Chi Zhang[1], Xin Li[1], and Junsheng Wang[1,2,*]

[1] School of Materials Science and Engineering, Beijing Institute of Technology, Beijing 100081, China
[2] Advanced Research Institute of Multidisciplinary Science, Beijing Institute of Technology, Beijing 100081, China

Received: 4 November 2020
Accepted: 3 February 2021
Published online: 24 February 2021

ABSTRACT

Nanoscale $\delta'/\theta'/\delta'$ composite precipitate, as another important strengthening phase in the latest generation of Al–Li alloys, exhibits excellent resistance to coarsening. Here, we propose two thickening models for an anomalous $\delta'/\theta'/\delta'$ that is discovered recently, by analyzing various influencing factors, including the static energy barrier, aging temperature-dependent nucleation conditions, and the elastic distortion suffered during growth. It indicates that the thickness of the $\delta'/\theta'/\delta'$ composite precipitate seems to depend on the nucleation of the δ'. At elevated aging temperatures, θ' precipitates can grow and thicken rapidly until the δ' nucleates on them. This is strikingly different from the dislocation-induced growth mechanism. Subsequently, we propose a vacuum-added methodology to accurately extract the interfacial energy. The results show that this nano-composite precipitate can realize supra-nanostructure in thickness at low aging temperatures due to the spontaneous nucleation of the δ' upon the pre-precipitate θ'. Cu atoms segregated at the interface suppress the nucleation of the δ', but release the lattice distortion to some extent. Using Griffith fracture model-assisted *ab-initio* uniaxial tensile tests, the cohesion strength and fracture process of this composite precipitate with and without Cu segregation have been captured. It indicates that the Cu atoms induced interfacial expansion and the fracture of strong Al–Al covalent bond, resulting in a reduction of fracture strength of this nano-composite precipitate.

Handling Editor: N. Ravishankar.

Address correspondence to E-mail: junsheng.wang@bit.edu.cn

https://doi.org/10.1007/s10853-021-05894-2

Introduction

Third- and fourth-generation Al–Li alloys as promising structure materials have broad industrial applications, owing to an excellent combination of high specific strength, high toughness, and satisfactory fatigue performance [1, 2]. Advanced nano-precipitation strengthening is of great technological importance to modern Al–Li alloys, being responsible for providing the required strength. In the past decades, the T_1 nano-precipitate as the most effective strengthening phase has attracted significant amounts of research efforts to favor its formation in Al–Li alloys through careful alloy design and thermomechanical processing [3–5]. Besides the T_1, nano-composite precipitates with the association of different precipitates, such as $\delta'/\theta'/\delta'$, θ'/β' and $\theta'/\delta'/\beta'$, have been commonly found in Al–Li alloys by adding Cu and Zr elements [6–8]. It is proven that the pre-precipitate θ' can serve as a preferential site for the nucleation of δ' and β' nanoparticles. Compared with single-phase precipitates, greater amount of energies would be required for dislocations to pass around these composite precipitates than individual δ' or θ' precipitates, separately. On the other hands, inter-phase boundaries (IB) within these composite precipitates are more resistant to dislocation movement due to the different crystal orientations and lattice parameters which can introduce crystallographic disregistries between the adjacent regions of constituent phases (planar defects). Therefore, the composite precipitates become another major source of strengthening phases and play an important role in contributing to the overall mechanical performance of Al–Li alloys.

Recently, the $\delta'/\theta'/\delta'$ nano-composite precipitate is attracting considerable attention in Al–Li alloys. Based on the analysis of atomic-resolution high-angle annular dark-field (HAADF) images in scanning transmission electron microscope (STEM) combined with density functional theory (DFT) calculations, its crystal structure, and the probable thickening mechanism have been proposed [7–11]. Interestingly, the thickening or coarsening of the θ' phase sandwiched by δ' phase on both sides is rather different from the conventional θ' precipitate in Al–Cu alloys. In this nano-composite precipitate, the θ' thickens by engulfing the sideward δ' precipitates, accompanied by a remarkable structure modification of the δ' at the interface. During the layer-by-layer growth of the inward θ', it was found that there existed two crystallographic relationships for the opposite δ', namely "anti-phase" and "in-phase", which can alternate for each other depending on the inward θ' with varying Cu-layers. This may be direct evidence of the chemical bonds of constituent atoms, which exhibits a regular arrangement at the IB [10]. According to minimal energy requirements, we subsequently found that this unique crystallographic relationship transition could be achieved by sliding one side of the δ' along the (001)[110] direction for $\sqrt{2}/2\,a$ (a is lattice parameter of this composite precipitate parallel to the IB) [10]. For this transformation, however, the θ' thickening with modification of the δ' to match the newly formed θ'/δ' interface structure will inevitably cause additional lattice distortions between the nano-composite precipitate and the α-Al matrix, which in turn restricts the thickness of the θ' precipitates. As a result, relatively thin $\delta'/\theta'/\delta'$ precipitates (3–4 nm in total thickness with only 2–6 Cu-layers) were always observed in experiments [7, 8, 11].

Regarding the recent report on this nano-composite precipitate, we noticed that the inward θ' can grow up to 39 Cu-layers with the overall thickness reaching 16 nm, which is far beyond the previous experimental observations [6]. Furthermore, it should be noted that the marginal δ' phases remain $\sim$ 2 nm throughout, therefore, the overall thickness of this nano-composite precipitate is mainly controlled by the inward θ', especially for very thick ones. At present, the thickening mechanism may be the only viable option for the thin $\delta'/\theta'/\delta'$. Whether the thick ones do by this way is still an open question. In fact, for those very small nano-composite precipitates, it is important to understand not only their size evolutions but also their number densities, since their ultimate effectiveness in preventing dislocation movements depends on their interactions with dislocations. Therefore, blocking dislocations movements by tailoring the $\delta'/\theta'/\delta'$ nano-composite precipitate may inspire new design principles for high-strength Al–Li alloys.

Before tailoring and optimizing the thickness of this nano-composite precipitate, we need to understand the underlying thickening mechanism of the inward θ'. In the case of single θ' precipitates in Al–Cu alloys, some investigators proposed that the θ'/α-Al interface with Cu segregations could be an

intermediate state in the thickening process of the θ' [12–14]. When interfacial segregation of Cu appears at the θ'/α-Al interface, it produces a GP(I)-like zone. Then, these Cu atoms diffuse to the adjacent Al matrix to generate the bulk structure of the next θ' unit cell. Inspired by this, the preferential segregation and the subsequent diffusion of Cu atoms in the IB of the $\delta'/\theta'/\delta'$ may be a potential measure to promote the growth of the θ', considering the similarity between θ'/α-Al and δ'/θ' interfaces.

This study aims to investigate the reason behind the thickness differences and the corresponding thickening modes of the $\delta'/\theta'/\delta'$ nano-composite precipitate by performing DFT calculations. Based on the precise solute-segregation-induced growth mechanism, two models have been proposed to explain the thickness variations by combining the energy barrier calculations during nucleation and growth thermodynamics under aging heat treatment. To accurately evaluate the heterogeneous nucleation of the post-precipitate δ', a vacuum-added (VA) methodology was proposed for the interfacial energy calculation. Using this methodology, the influence of Cu segregations on δ' nucleation was evaluated. Hereafter, a canonical Griffith model [15] and *ab-initio* uniaxial tensile tests were combined to evaluate the cohesion strength and fracture characteristics of the $\delta'/\theta'/\delta'$ with and without segregated Cu atoms. The final fracture interface was also examined from multiple angles. In the last part, the electronic structures were utilized to analyze the underlying effects that Cu solutes played in embrittling the IB of the $\delta'/\theta'/\delta'$. Our present theoretical calculations provide not only a fundamental understanding of the thickening mechanism of the $\delta'/\theta'/\delta'$ nano-composite precipitates but also useful guidance for the development of high-performance Al–Li alloys by regulating the size of $\delta'/\theta'/\delta'$ nano-composite precipitates in the future.

Methods and models

First-principle calculations

For all calculations, including the structural relaxations, electronic self-consistent iterations, and the related derivatives were performed using the *Vienna* ab-initio *simulation package* (VASP) [16]. The generalized gradient approximation (GGA) in the Perdewe–Burke–Ernzerhof (PBE) form was utilized to describe the electronic exchange and correlations [17]. Brillouin zone integrals were performed over a k-point grid of the density at 0.03 (in the unit of $2\pi/$Å) using Monkhorst-Packset sampling [18]. An energy cutoff of 600 eV was sufficient for setting up plane wave basis. The self-convergence accuracy of the iterative was set at less than 1×10^{-5} eV/atom and 0.02 eV/Å for forces.

Interphase boundaries and energetics

In this work, a representative $\delta'/\theta'/\delta'$ nano-composite structure with five Cu-layers was constructed based on unique interfacial terminations at the IB that were discussed in our previous report [10]. Figure 1a represents the atomic structures of this $\delta'/\theta'/\delta'$ with a full separation of solute atoms Z at the IB. In each interfacial supercell, it contains seven layers of (001) planes of the δ' stacking in the direction perpendicular to the IB, and an "in-phase" characteristic presents due to the periodicity. For these segregation sites along the IB, they are the most spatially favorable ones that were obtained similar to the θ'/α-Al interface [14].

Prior to evaluating the heterogeneous nucleation and growth behaviors of the post-precipitated δ' phase, we calculated the corresponding interfacial energy γ_{inf}, where the interface δ'/θ' is modeled as an atomically sharp junction between bulk δ' and θ' phases. Generally, the γ_{inf} can be quantitatively evaluated by two approaches, namely linear fitting (LF) and direct calculation (DC) [19, 20]. For the former, it is considered that the γ_{inf} is only proportional to the cross-sectional area of the supercell. By fitting the energy of formation per atom ΔE_{f} *v.s.* $1/N$ (N is the total number of atoms in the supercell), the slope of this fitted line will be the interfacial energy γ_{inf}. Here, the ΔE_{f} can be written as follows:

$$\Delta E_{\text{f}} = \frac{1}{N}\left[E_{\text{A/B}} - N_{\text{A}}E_{\text{A}} - N_{\text{B}}E_{\text{B}} - \sum_i l_i\mu_i\right] \quad (1)$$

where $E_{\text{A/B}}$, E_{A}, and E_{B} are the total energy for the interfacial supercell, bulk A and B phases, respectively. N_{A} and N_{B} are the number of formula units of bulk A and B phases in this interfacial system. In the case of an off-stoichiometric interfacial system, whose stoichiometry is not commensurate with the bulk, μ_i corresponds to the chemical potential of extra atoms with a number of l_i. In the present work, δ' and θ' are

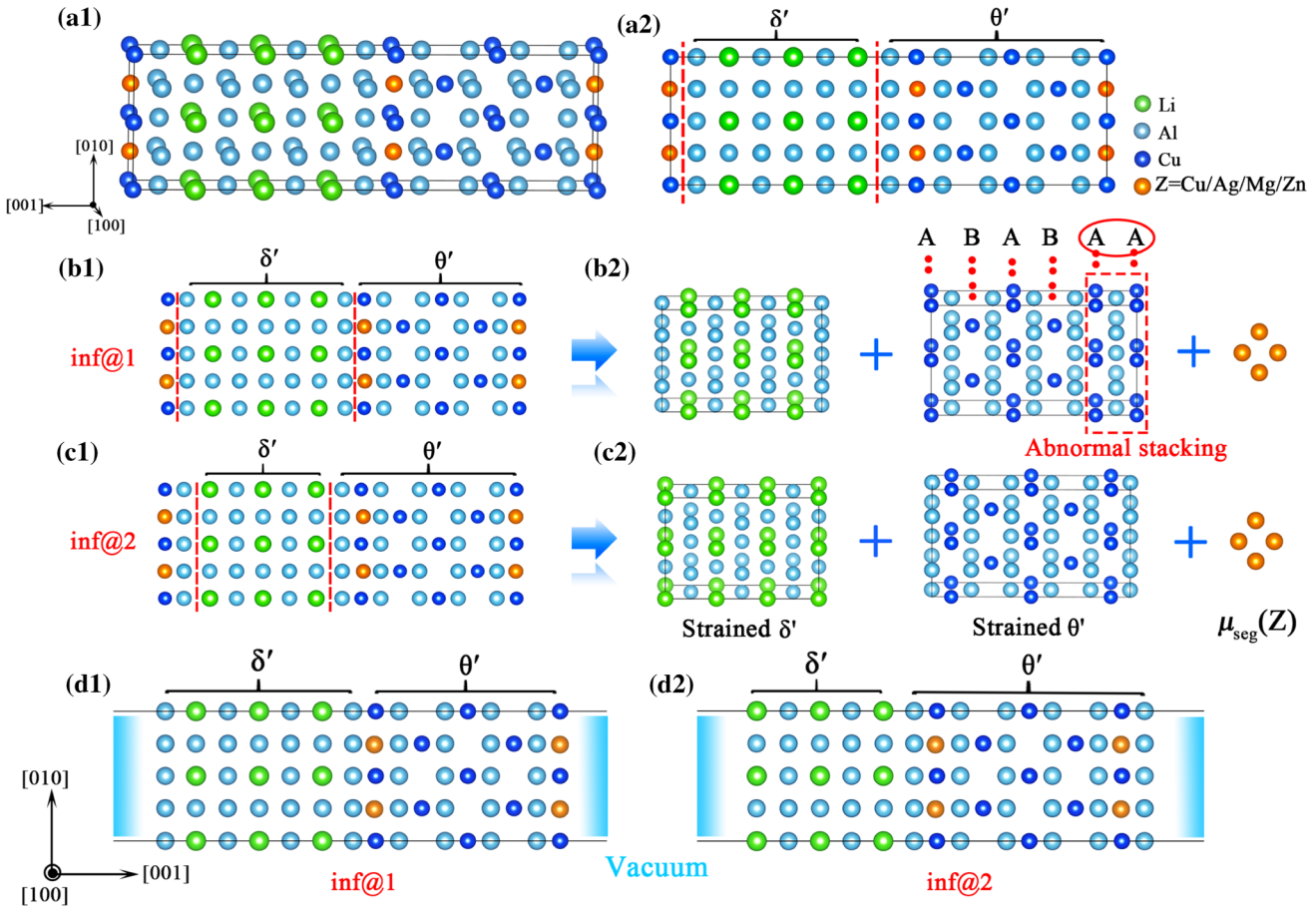

Figure 1 **a1** The atomic structure of the $\delta'/\theta'/\delta'$ nano-composite precipitate with alloy segregations at the interface. **a2** Asymmetrical interface structures due to phases division by six bulk δ' and ten bulk θ', as discussed in the text. **b1** and **c1** are the interfacial models inf@1 and inf@2 with chemical segregation at the interfaces, respectively. **b2** and **c2** show schematics of calculating the interfacial energy γ_{inf} for the inf@1 and inf@2 interfaces using direct calculation (DC) methodology, respectively. An abnormal stacking of the Cu-layer occurs in the θ' phase using the DC methodology (shown in the dotted red box). μ_{seg} represents the chemical potential of the segregation elements Z. **d1** and **d2** are the vacuum-added interfacial supercells for constructing the inf@1 and the inf@2, respectively.

A and B phases in Eq. (1), respectively, and N_A (N_B) is balanced by the number of Li (Cu) atoms in the δ' (θ'). Subsequently, we will have six bulk δ' phases (with a stoichiometry of Al_3Li), and ten bulk θ' phases (with a stoichiometry of Al_2Cu). If the interface is divided by the amount of the atoms corresponding to the above bulks, it will result in a physically unreasonable one as the red dotted line indicated in Fig. 1b2. Fortunately, considering that the chemical potential of Al must be the same among the δ' (μ_{Al} (δ')), θ' (μ_{Al} (θ')), and Al matrix (μ_{Al} (matrix)) in local equilibrium, otherwise the system could lower its total energy by transferring Al atoms from one phase to the others. Therefore, a solvable interface can be obtained from the perspectives of the structure and energy. For example, there are two types of interfacial models as shown in Fig. 1b1 and c1, namely inf@1 and inf@2, respectively. Based on the above inference about the chemical potential of Al atoms, we find that both types of interfaces will share the same or average interfacial energy values. Obviously, this would make it confusing to precisely define the nucleation of the δ' on θ'-precipitates from the point of view of the nucleation position, and the associated thermodynamics of the nucleation, i.e., the interfacial energy. This also becomes challenging for the subsequent discussion on the potential influence of interstitial Cu atoms on this heterogeneous nucleation.

As a simplification, the DC methodology is usually applied to extract the γ_{inf} of a large interfacial supercell. In general, this calculation process can be

divided into several parts: first, the interfacial supercell is separated into specified parts according to the interface object. Then, the stress-free bulk components are deformed to the same structures as in the interfacial structure, respectively. For interfacial structures with atomic segregation, the chemical potentials of segregation atoms μ_{seg} can be obtained by an approximate calculation based on a dilute solid solution model, and the specific details are described in "Thickening models" section. Since there is no lattice distortion, the energy difference before and after deforming the components only constitutes the interfacial energy γ_{inf}. Using this methodology to calculate the inf@1 interfacial energy γ_{inf}, however, we obtained an abnormal structure, as shown inside the dotted red box in Fig. 1b3, when we tried to balance the number of atoms in the strained θ' phases with those contained in the interfacial supercell. This obviously destroys the stacking sequence of the θ' along the (001) direction as shown in Fig. 1b1. Consequently, the DC methodology failed again.

Inspired by the above two methodologies, if we want to obtain the interfacial energy γ_{inf} accurately, first of all, we cannot use the general idea of equating the amounts and classes of atoms contained in the interfacial structures with those in the constituent phases. This would produce ambiguous interfaces that have the same energy but completely different structures. Secondly, the interfacial supercells should be constructed with fewer periods to ensure that the heterogeneous interface is unique. Especially for constituent phases with complex stacking configuration, uniform interfaces are often more difficult to achieve in periodic structures. To achieve this goal, we performed a vacuum-added (VA) methodology to separate the interface of interest by introducing extra but relative surfaces for the new one, as shown in Fig. 1d. Specifically, we carried out the separation of the γ_{inf} using the following process: first, we performed a full geometry optimization of this interfacial supercell including atomic positions and cell vectors, and we obtained ground lattice vectors **a**, **b**, and **c** (where vectors **a**, **b** lie in the interfacial plane, while vector **c** is normal to the plane) with total energy denoted as $E(\delta'/\theta')$, which is equal to:

$$E(\delta'/\theta') = \sum_i \mu_i(\text{bulk} + \text{solute}) + 2 \cdot S \cdot \gamma_{inf}(\text{inf}\,@x) \quad i = \delta', \theta', Z; \quad x = 1, 2 \tag{2}$$

where μ_i is the chemical potential of the δ', θ' bulks, and solute atoms Z. S is the interface area. Second, the static energy of the vacuum-added interfacial supercell was calculated while retaining the same cell vectors and atomic positions. At this point, the total energy calculated is denoted as $E(\delta'/\theta'\text{-vac})$, which can be broken down further into the following components:

$$E(\delta'/\theta' - \text{vac}) = \sum_i \mu_i(\text{bulk} + \text{solute}) + \left[\gamma_{inf}(\text{inf@x}) + \sum_j \gamma^j_{suf}(\text{inf@x})\right] \cdot S \quad j = \delta', \theta' \tag{3}$$

where the γ^j_{suf} is the additional surface energy introduced by vacuum at the edge of the interfacial supercell, and other variables, are the same as in Eq. (2). Cleary, in the vacuum-added interfacial supercell, the structural features of δ' and θ' phases, including the interface, atomic compositions, and atomic segregations are the same as the initial ones, that is, the first terms on the right side of Eqs. (2) and (3). The total energy difference of the interfacial supercell before and after the introduction of vacuum can be written as follows:

$$\Delta E = \left[\gamma_{inf}(\text{inf@x}) - \gamma^{\delta'}_{suf}(\text{inf@x}) - \gamma^{\delta'}_{suf}(\text{inf@x})\right] \cdot S \tag{4}$$

Clearly, the ΔE, $\gamma^{\delta'}_{suf}(\text{inf@x})$, and $\gamma^{\theta'}_{suf}(\text{inf@x})$ are easy to be calculated using DFT, the surface energy is approximated by a general way, see Ref. [21] for details. Once the γ_{inf} is obtained, the corresponding strain energy δ per atom can be easily calculated as follow:

$$\delta(\text{inf@x})/N = \Delta E_f - 2 \cdot \gamma_{inf}(\text{inf@x}) \cdot S/N \tag{5}$$

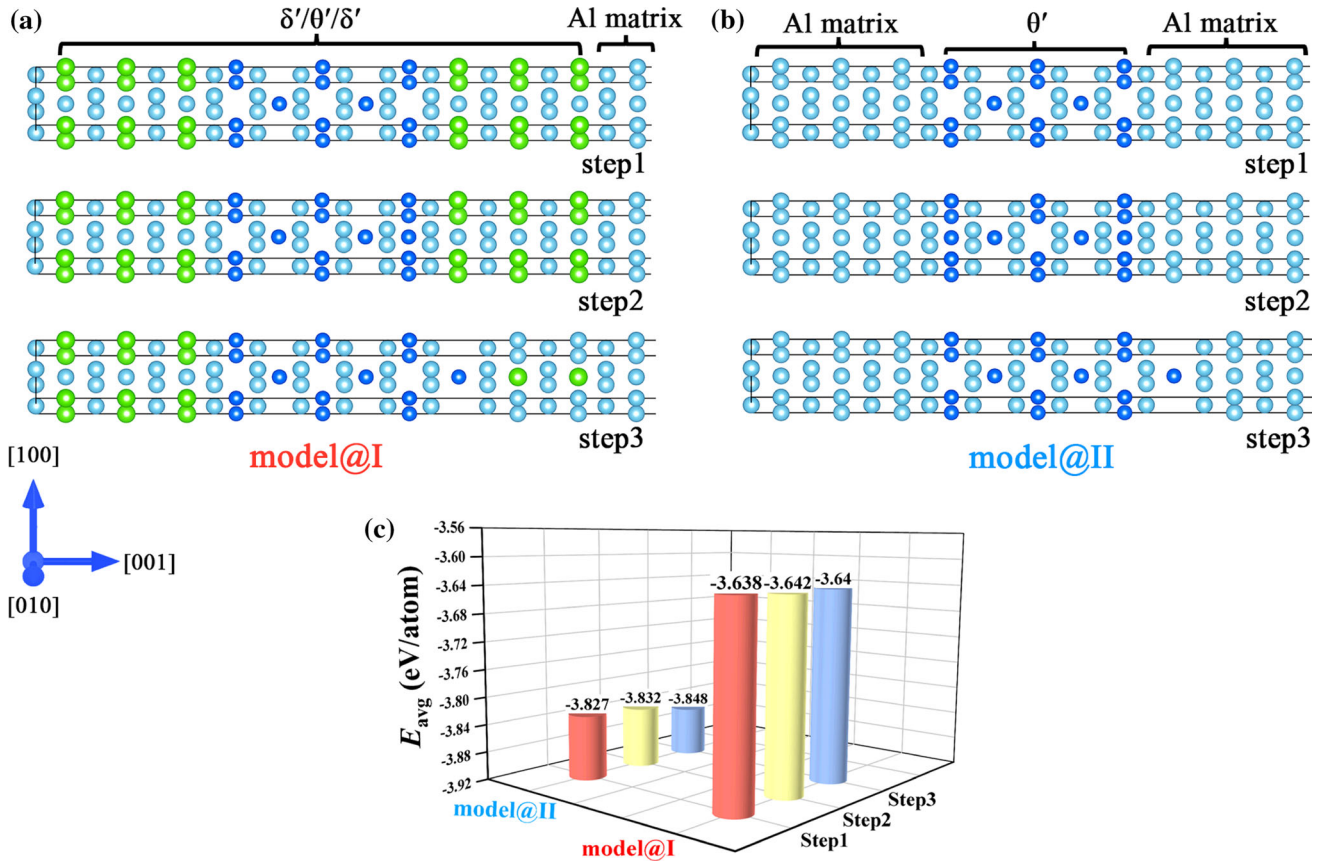

Figure 2 Two types of thickening models for the $\delta'/\theta'/\delta'$ nanocomposite precipitate with centered θ' phases growing from $2c_{\theta'}$ to $2.5c_{\theta'}$ via a $0.5c_{\theta'}$ ledge. **a** The θ' phase grows within the $\delta'/\theta'/\delta'$, denoted as Model@I. **b** The θ' grows in the α-Al matrix, denoted as Model@II. (c) The average effective energy E_{avg} of all interfacial supercells during thickening.

Results and discussion

Thickening models

Model@I and model@II for thickening

To understand the difference in thickness of the $\delta'/\theta'/\delta'$, two types of thickening models have been constructed for illustration, corresponding to different growing environments for the θ' phase. The entire processes of two models from conception to completion are shown in Fig. 2. The first model is α-Al/$\delta'/\theta'/\delta'$/α-Al that is used to describe the θ' growing inside the $\delta'/\theta'/\delta'$, namely model@I in Fig. 2a. The second model is a classical α-Al/θ'/α-Al interface, designated model@II in Fig. 2b. For both models, the thickening of the centered θ' phases is from $2c_{\theta'}$ to $2.5c_{\theta'}$ via a $0.5c_{\theta'}$ ledge to simulate a normal growth process. To obtain the energy evolution of these growth processes, we consider average effective energy, which is calculated as the total energy divided by the total number of atoms, defined as E_{avg}. The total energy involves composition from elements consisting of the same number of atoms. For example, at step1, the interfacial supercell does not have interstitial Cu atom segregations, and the contribution of those active Cu atoms is considered to be the chemical potentials of Cu atoms that are distributed evenly in Al matrix. To evaluate the chemical potential of one Cu atom, a supercell ($3 \times 3 \times 3$ with 108-Al atoms in total) is constructed, then we replaced one Al site with Cu randomly to form a Cu-doping dilute solid solution. Clearly, this solubility is well below the limit of Cu in Al matrix. Taking a similar approach, the chemical potential of Li atoms has been evaluated for the corresponding $\delta'/\theta'/\delta'$ in step3.

Figure 2c shows the average energy E_{avg} of relevant interfacial supercells presenting the thickening process. For the model@II, there is a monotonical decrease in the E_{avg} as the θ' phase finishes the

specified growth gradually. From step1 to step2, the spontaneous aggregation of Cu atoms at interstitial sites forms a GP-like zone, which proves a good agreement with previous experiments and theoretical reports [14]. As the θ' phase is grown from step2 to step3 by diffusions of Cu and Al atom, it can be described as a spontaneous transformation due to the reduction of free energy. Therefore, we can conclude that the θ' phase with Cu segregation possesses a robust potential to become thicker and coarser without an additional driving force. However, for the model@I, this process does not seem to be as straightforward as model@II. From step1 to step2, there is also a negative gradient of the average energy E_{avg}, which provides evidence for supporting the presupposition of the model@I in $\delta'/\theta'/\delta'$, whereas when these segregated Cu atoms diffuse to the adjacent δ' to finish the step3, we find that there is an energy barrier, which does not even include the driving energy to overcome the arising lattice distortion caused by the δ' rearrangement. As a result, although the interstitial Cu atoms are observed at the interfaces and not in the bulk of the precipitate, we believe that for a much thick $\delta'/\theta'/\delta'$, the θ' phase should not be covered by δ' phases before the end of its growth stage. Once δ' phases nucleate and grow at the edge of the pre-precipitate θ', they can restrict its growth, resulting in thin θ' precipitates. This might explain the fact that the thickening θ' precipitates were not frequently observed, but the lengthening ones were usually captured after aging treatment in previous experiments, whereas for θ' particles which are not covered by the δ', they can freely thicken and lengthen, leading to rather coarse θ' plates eventually.

Aging temperature-dependent thickening models

To discover the thickening mechanism from nucleation conditions, aging time and aging temperatures controlling the formation of $\delta'/\theta'/\delta'$ nano-composite precipitates have been summarized and compared from the extensive literature reviews [6–9, 11]. Although the aging time is an important parameter, we find that it has a very slight impact on the thickness of the θ' within $\delta'/\theta'/\delta'$ composite precipitates. The thickness of the θ' phase is strong function of aging temperatures. Specifically, when temperature range is between 165 and 190 °C, the thickness of the θ' phase is only 0.5−3 nm. As increasing the aging temperature, the θ' phase grows to $\sim$ 5 nm at 250 °C. When the aging temperature is up to 350 °C, there will be $\sim$ 14 nm θ' precipitates in thickness. This clearly demonstrates the temperature dependence of the θ' thickness. Generally, the metastable δ' phase has lower thermal stability and poorer coarsening resistance than the θ' phase [22, 23]. Taking experiences from previous works on the δ' in high-Li Al–Li alloys, we know that its ordering transformation is through congruent ordering + spinodal decomposition at $\sim$ 140 °C [24]. In consideration of the so strong temperature-dependent solubility and mobility of Li atoms in Al–Li alloys, it is difficult to have spinodal decompositions following congruent ordering to form the δ' at high temperature. This is the reason why its volume fraction is reduced as well as atomic disordering occurs at temperatures above 200 °C. Therefore, it constitutes that in the early stage, where the δ' envelopes are absent, the θ' phases rapidly grow in thickness at high temperatures (over 200 °C). By contrast, at relatively low temperature, δ' phases will nucleate and further grow on the θ' phase, which leads to a significant growth restriction to the θ' phase before the dissolution of the δ' phase.

According to the above discussion, we know that these two types of growth channels of the θ' cause different $\delta'/\theta'/\delta'$ nano-composite precipitates in thickness. They are closely related to aging temperatures in the actual heat treatments. In model@1, δ' phases nucleate on the pre-precipitate θ' at low aging temperature, leading to a relatively thin $\delta'/\theta'/\delta'$ composite precipitate after aging treatment. On the contrary, in model@2, the θ' phase shows a rapid growth and thickening at high aging temperatures. As the δ' starts to nucleate and grow on the θ', the thickening of the θ' phase is suppressed. Clearly, this is not in line with the previous conclusions that the growth of the $\delta'/\theta'/\delta'$ composite precipitate must involve dislocations with Burgers vectors $a/2[100]$ and $a/2[010]$ [7, 25]. Meanwhile, nearly no dislocations were found on the edges of these thickening precipitates in the existing experiments, which seems to confirm this thickening mechanism.

Nucleation and interfacial energy

Interfacial energy of the inf-free predicated via the VA methodology

Based on the above results, we know that the thickness of the $\delta'/\theta'/\delta'$ composite precipitate depends on

the nucleation stage of the δ' to a great extent. Actually, the nucleation rate and kinetics could directly determine whether the δ' can nucleate on the θ' phase or not. According to the classical nucleation theory, cell nucleation needs to overcome the energy barrier, which is proportional to the interfacial energy γ_{inf}.

Unlike normal precipitates that have a distinct interface with matrix, in the $\delta'/\theta'/\delta'$ composite precipitate, the interface between the two phases is vague due to the presence of a common Al-layer which is owned by both phases. When this Al-layer is divided differently, there are two very different nucleation sites for δ' phases (inf@1 corresponds to less Al-layer for θ' and more Al-layer for δ', while the inf@2 is opposite). Clearly, this is not realistic and even leads to errors in distinguishing the δ' nucleation. In addition, using the current two methods, namely LF and DC, to calculate the γ_{inf}, we have confirmed that they possess varying degrees of insufficiencies in energy solution and structure delineation. Therefore, in the following sections, we will use the VA methodology as introduced in "Interphase boundaries and energetics" section to calculate the interfacial energy γ_{inf} of the $\delta'/\theta'/\delta'$, including the inf@1 and the inf@2.

For a clear interface without interstitial atoms, namely inf-free, there is a large difference in the interfacial energy between two interfaces (Table 1, the corresponding calculation results of the surface energy are summarized in Table S1). If the positive and negative values are used as the criteria for identifying the nucleation of the δ' phase, the results obtained will be subversive. For the inf@2, it has small negative interfacial energy, suggesting that a sharp interface can form favorably between those. If the inf@2 serves as nucleation sites for the δ', it leads to a surprising conclusion that the nucleation process of the δ' upon the θ' is a spontaneous reaction with lowering the free energy of the system entirety. More significantly, the $\delta'/\theta'/\delta'$ nano-composite precipitate can realize supra-nanostructure in thickness by a normal aging treatment (below 200 °C). This may provide new knowledge to strengthening Al–Li alloys.

Interfacial energy of the inf-Cu interface predicated via the VA methodology

According to the discussion in "Thickening models" section, we learn that the interstitial Cu atoms can maintain at the interface of the $\delta'/\theta'/\delta'$ until the barrier of thickening, which relies on atomic diffusion, can be overcome. So, it is necessary to study the interfacial segregation of Cu atoms because the γ_{inf} of this precipitate–precipitate interface is strongly influenced by the chemical composition, which thereby affects the nucleation of the δ'. Prior to this, the segregation behavior of Cu atoms is evaluated by segregation energy ΔE_{seg}, and the common alloying elements presenting in Al–Li alloy are also considered for comparison. A detailed explanation of the segregation energy calculation method is described in Ref. [26]. As shown in Table 1, inf-Cu interface has negative segregation energy compared to the inf-free, indicating that Cu does preferentially segregate at the interface. Compared with other solute atoms further, only Cu atoms have segregation opportunities at this interstitial site, which seems to imply that the $\delta'/\theta'/\delta'$

Table 1 Segregation energy ΔE_{seg}, interface formation energy per atom ΔE_f, coherent strain energy δ, and interfacial energy γ_{inf} predicted via vacuum-added (VA) and direct calculation (DC) methodologies of interfaces inf@1 and inf@2 in the $\delta'/\theta'/\delta'$ composite precipitate with and without alloy segregations

Structure	Interface	ΔE_{seg} (eV/atom)	ΔE_f (KJ/mol)	γ_{inf} (J/m^2)[a]	δ (KJ/mol)[a]	γ_{inf} (J/m^2)[b]
inf-free	inf@1	–	0.658	− 0.008	0.722	–
	inf@2			− 0.041	0.959	− 0.108
inf-Cu	inf@1	− 0.038	0.941	0.058	0.548	–
	inf@2			0.025	0.768	− 0.059
inf-Ag	inf@1	0.277	2.449	0.261	0.648	–
	inf@2			0.248	0.731	0.160
inf-Mg	inf@1	0.476	3.770	0.478	0.503	–
	inf@2			0.451	0.688	0.362
inf-Zn	inf@1	0.375	3.098	0.360	0.663	–
	inf@2			0.351	0.724	0.257

[a]Vacuum-added methodology

[b]Direct calculation methodology

grown in model@I will possess the ability to remove impurities.

Considering the γ_{inf} of the Cu-segregated interfacial structure, i.e., inf-Cu, we can see that both interfacial energies of the inf@1 and the inf@2 will increase with respect to those in the inf-free case. Clearly, these Cu-segregated interfaces will pose certain difficulties for the δ' nucleation. For interfacial structures segregated with other alloying elements, including inf-Ag, inf-Mg, and inf-Zn, their interfacial energies have tremendous increases for both types of interfaces. It suggests that if these atoms segregate at the interface, they all make the δ' nucleate difficult on the θ' phase. In contrast to the γ_{inf}, the coherent strain energies of inf@1 and inf@2 decrease with the segregation of considered atoms for all interfacial structures, especially for the inf-Mg, as shown in Table 1. These segregation atoms release the localized residual stress, thus decreasing the elastic strain energy. It is similar to the function of segregation elements acting in many twin boundaries [27, 28]. For the same interfacial structure, when the common Al-layer is divided in different ways, the volume of each constituent phase will be changed. It is well known that the θ' has a bigger bulk modulus than the δ' [29, 30] and exhibits relatively strong resistance to deformation. When the total volume remains constant, the larger the volume change of the θ', the greater the total coherent strain energy of this interfacial structure would have. So, we can always get bigger strain energy in the inf@2 instead of the inf@1, as shown in Table 1.

Comparison of the interfacial energy via the DC and VA methodologies

In addition, we also performed the DC methodology to calculate the interfacial energy of the inf@2 for all interfacial structures to compare with the results calculated by the VA methodology. As shown in Table 1, the results calculated by two methodologies are clearly biased, and the γ_{inf} using the VA method is always overestimated by 60–100 mJ/m^2. However, when the segregated-free states are set to zero for reference, the differences $\Delta\gamma_{inf}$ from two methodologies show a good agreement and the error is within 21 ± 4 mJ/m^2. These relatively stable and small errors indicate that the effects of segregations on the δ' nucleation can be accurately assessed by these two methods. Therefore, it can be confirmed that the VA methodology proposed in this work is feasible and applicable to the calculations of the γ_{inf} for complex interfacial structures (Fig. 3).

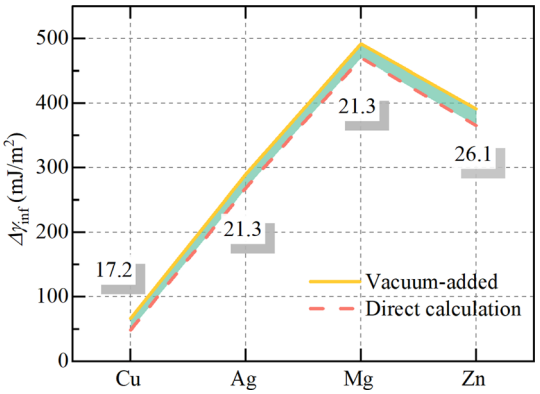

Figure 3 The scaled interfacial energy $\Delta\gamma_{inf}$ calculated using the vacuum-added (VA) and direct calculation (DC) methodologies. The $\Delta\gamma_{inf}$ refers to the difference of interfacial energy of the interfacial structure with and without segregation atoms.

Interface strength of the $\delta'/\theta'/\delta'$ with Cu segregations

First-principles-based tensile tests

To shed light on the influences of Cu segregation on the strength and fracture behavior of the $\delta'/\theta'/\delta'$ nano-composite precipitate, a canonical Griffith model (all Cu atoms reside at fractured surfaces come exclusively from the IB interface following the cracking process) and *ab-initio* uniaxial tensile tests are combined to capture the cohesion strength and the fracture by using the rigid grain shift (RGS) and the RGS + relaxations methods [31, 32]. Under uniaxial tension, the equilibrium structures are shifted in the direction normal to the pre-defined interface with an increasing vacuum gap distance. For RGS, it simulated the brittle cleavage in loading mode I without atomic relaxations as expected. For RGS + relaxations, atomic positions are allowed to relax, thus releasing the elastic energy. For both methods, the total elongation of the interfacial structure remains constant without Poisson's contraction in other directions. After obtaining a set of energy-displacement data via the RGS method, the so-called universal binding energy relation (UBER) [31] is used to fit these displacement-dependent separation energies according to the following equations:

$$E_b(d) = \left|E_b^e\right| \cdot g(a) \tag{6}$$

$$g(a) = -(1+a) \cdot e^{-a} \tag{7}$$

where E_b^e is the binding energy at equilibrium, d is the displacement, and a is the rescaled displacement defined as, $a = d/l$, where l is a characteristic length as follow:

$$l = \sqrt{\frac{\left|E_b^e\right|}{E_b''(d_0)}} \tag{8}$$

The work of separation W_{sep} of an interface ($= -\left|E_b^e\right|$ at equilibrium volume) is defined as the energy penalty required for the intergranular fracture of an interface into two free surfaces and can be calculated via the following equation [33]:

$$W_{sep} = \gamma_{suf}^{\delta'}(\text{inf } @x) + \gamma_{suf}^{\theta'}(\text{inf } @x) - \gamma_{inf}(\text{inf } @x) \tag{9}$$

Actually, it shows an opposite expression as compared with the ΔE in Eq. (4), suggesting that the VA methodology can provide direct guidance to the W_{sep} requiring no further calculations of the surface energy. However, it should be noted that the coherent strain energy is not included in this special W_{sep} calculated by the VA methodology. The ΔE_f of the inf@1 and the inf@2 is equivalent using the LF methodology. In this case, the VA methodology is not a feasible solution for calculating the W_{sep}. Therefore, in the following sections, we use the DC methodology to calculate relative binding energy. For the RGS + relaxation calculation, a fifth-order polynomial is used to fit the energy-displacement data where the displacement is below the critical displacement l_h, which represents the upper limit of restorability due to elastic relaxations under uniaxial tensile.

Confirmation of the fracture interface

Before investigating the brittle fracture of this interfacial structure, it should be noted that for both tensile methods, the vacuum spacing between two blocks of atoms increases only at a pre-defined cleavage interface. Whether this is the case for the final pattern remains to be verified. Based on the results on the interfacial energy in "Nucleation and interfacial energy" section, the inf@2 may be identified as the final breaking one since its smaller and negative γ_{inf} than that of the inf@1, regardless of the presence of Cu atoms segregated in the $\delta'/\theta'/\delta'$ composite precipitate.

On the other hands, using the RGS + relaxation method to relax all pre-defined fracture interfaces, we can obtain the most likely one. As shown in Fig. 4, the final fracture surfaces after relaxation are always split along the inf@2, in which the common Al-layer attributed to the θ' maintains almost the same interplanar spacing and arrangement as in the bulk structure. Actually, this conclusion can also be supported from the perspective of nucleation process analysis. In terms of the δ', we know that it nucleates and grows on the pre-precipitate θ'. As the Li atoms move into the specific lattice sites of the ordered $L1_2$ structure to form the δ' [34], in fact, this Al-layer exists prior to Li atoms diffusion. Therefore, we set the inf@2 as the fracture interface in the following discussion.

Theoretical tensile strength

Figure 5a displays the rescaled binding energy-displacement curves of the inf@2 in two interfacial structures of the inf-free (denoted as inf-free@2) and the inf-Cu (denoted as inf-Cu@2) evaluated via the RGS method. It can be seen that these rescaled results follow the UBER fitting curves very well. Comparing the values of the E_b^e shown in Fig. 5a and Table 2, the inf-free@2 has a relatively small one, which is about 3.8% less than that of the inf-Cu@2. On the other hands, according to the relationship between the E_b and the W_{sep}, the inf-free@2 will have a large W_{sep}. It suggests that the inf@2 possesses a slightly weak resistance to interfacial fracture when there are Cu atoms segregated at the interface. Again, this result can be confirmed by the tensile strength analysis from Fig. 5c and Table 2. As both interfacial structures are stretched to the critical separation δ_c, the theoretical strength of the inf-free@2 is as high as 14.22 GPa, which is ~ 18% larger than that of inf-Cu@2 (12.05 GPa). Apparently, these Cu solutes segregated at the interface appear to be cohesion suppressors of the $\delta'/\theta'/\delta'$ nano-composite precipitate. In addition, comparing the results of the W_{sep} evaluated through two ways corresponding to Eqs. (4) and (9), we can find that the strain energy contributes little to the ΔE_f due to the difference of the W_{sep} is only 3.8–3.9%, as listed in Table 2.

These rescaled binding energy curves can be divided into three distinct regions for the relaxed-type

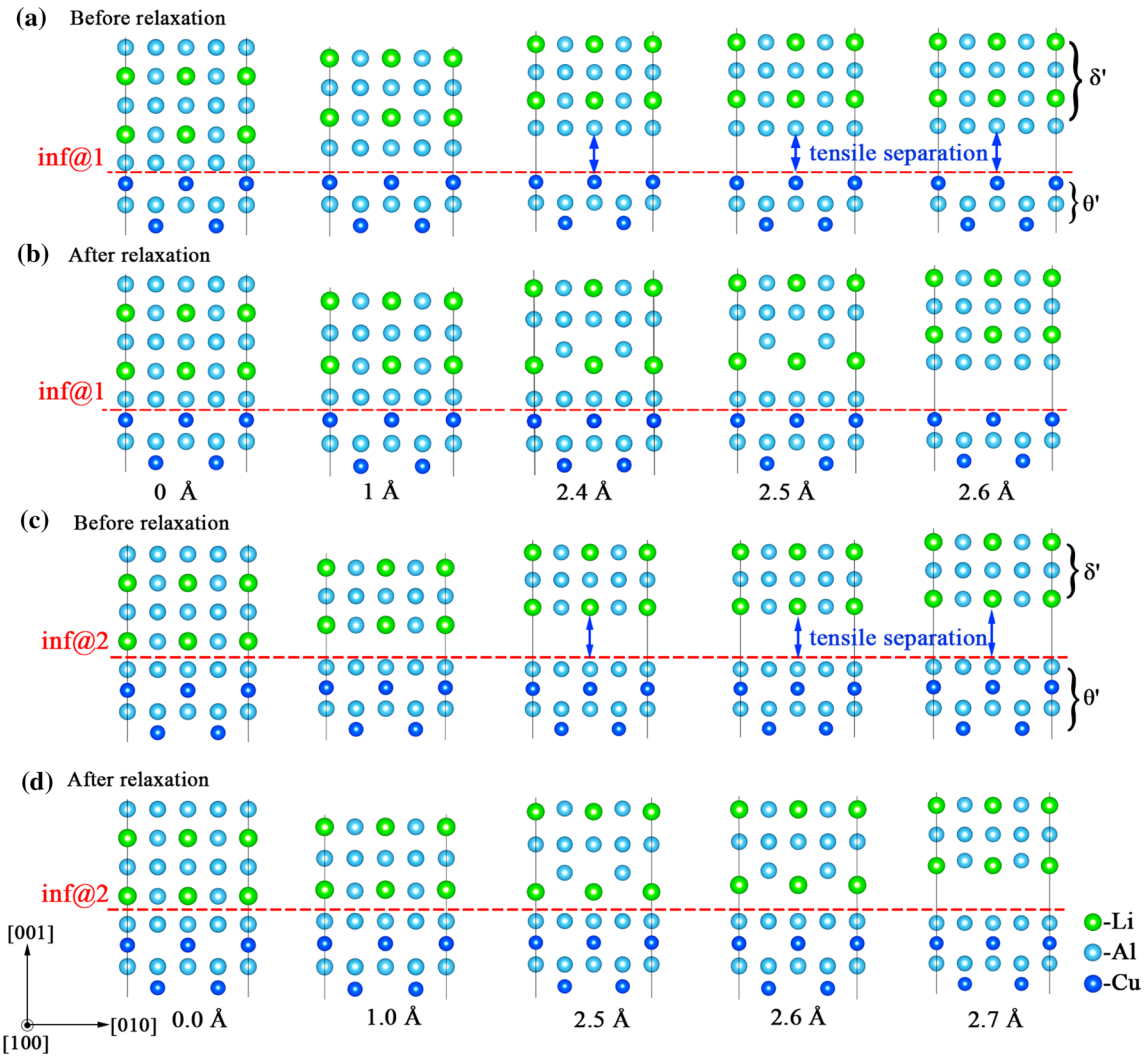

Figure 4 Interfacial structures of the inf@1 and the inf@2 before and after relaxation via the RGS + relaxation method. **a**, **b** show the interfacial structures before relaxation, while **b**, **d** show the structures after relaxation.

tensile tests, as shown in Fig. 5b. When the displacement is smaller than the l_h ($\delta < l_h$), the pre-crack introduced during tensile separation can be healed up after elastic relaxations. As the crack opening increases, between $l_h < \delta < l_f$, the pre-crack can neither be healed up nor be separated completely as free surfaces, being a so-called instability region. When the displacement is over the l_f, the preset fractured interfaces are unchanged and the corresponding surfaces are completely separated. As shown from Fig. 5b, the fracture of the inf-Cu@2 is completed at the displacement of 2.5 Å, which is 0.1 Å in advance than that of the inf-free@2. Meanwhile, the theoretical strengths of the latter can reach 12.25 GPa, which is about 20% larger than that of the former. Though the theoretical strength is always underestimated by the RGS + relaxation approach, which represents the overall strength of the simulation supercell, the weakening effect of the Cu atoms segregation on $\delta'/\theta'/\delta'$ composite precipitates could be verified.

Charge density

To further understand the weakening effect of Cu atoms segregated at the IB of the $\delta'/\theta'/\delta'$ nanocomposite precipitate, we investigated the relevant charge density evolution during uniaxial tensile processes. As shown in Fig. 6, for the inf-free, two types of covalent bonds are formed at the interface after atomic relaxations, including strong Al–Al bonds and weak Al–Li bonds. Obviously, these strong Al–Al bonds contribute primarily to the

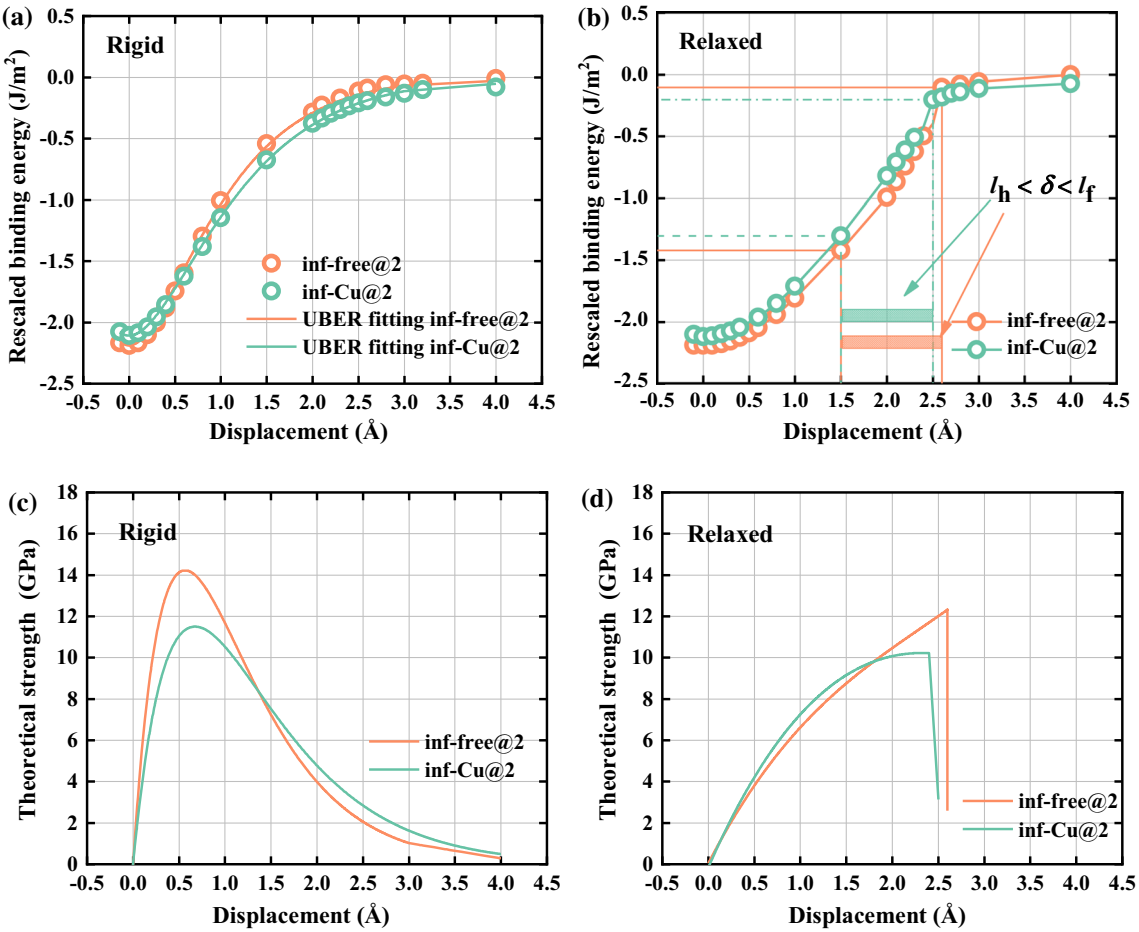

Figure 5 The rescaled binding energy and tensile stress as a function of the separation distance for the inf@2 in inf-free (labeled as inf-free@2) and inf-Cu (labeled as inf-Cu@2) interfacial structures. **a** The rescaled binding energy versus displacement curves evaluated via rigid grain shift (RGS) method and fitted by the UBER. **b** The rescaled binding energy versus displacement curves evaluated via rigid grain shift (RGS) + relaxation method. The shadow area represents the instability region δ of interval crack openings between l_h and l_f, where l_h represents the critical displacement. Below this the crack can be healed via elastic relaxations, while cracks form after displacements beyond l_f. **c** Stress–strain curves plotted by differentiating the UBER curves given in (**a**) from the RGS method, and **d** using the UBER + relaxation method given in (**b**).

Table 2 The ideal work of separation W_{sep} of the inf@2, evaluated by the vacuum-added (VA) and the direct calculation (DC) methodologies, critical separation δ_c, and fracture strength σ_{th} predicted via rigid grain shift (RGS) and RGS + relaxation methods

	W_{sep} (J/m^2)[a]	W_{sep} (J/m^2)[b]	δ_c (Å)	σ_{th} (GPa)[c]	σ_{th} (GPa)[d]
Inter-free	2.19	2.14	0.59	14.22	12.25
Inter-Cu	2.11	2.06	0.66	12.05	10.21

[a]Direct calculation methodology

[b]Vacuum-added methodology without strain energy

[c]RGS method

[d]RGS + relaxation method

breaking strength of the $\delta'/\theta'/\delta'$ at the ground state. However, these two types of bonds show different trends as the separation distance d increases. When d reaches 2.4 Å, a depletion region of the charge density appears suddenly between these strong Al–Al bonds, causing them to weaken rapidly. On the

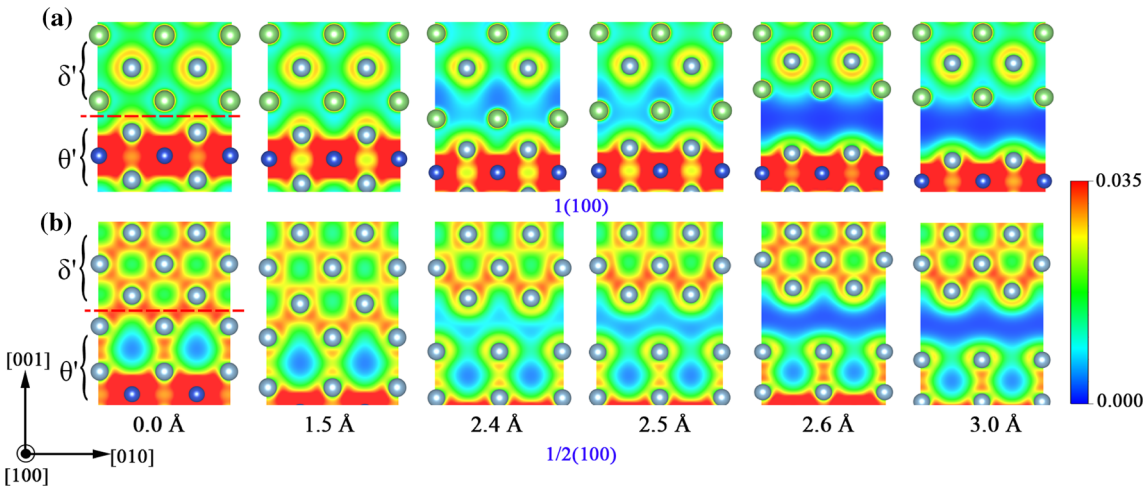

Figure 6 Charge density distributions of the inf-free in 1(100) and 1/2(100) planes along with an increased displacement distance (in Å) shown below each frame, using the RGS + relaxation method. The unit is in e/Bohr^3.

contrary, those relatively weak Al–Li bonds remain basically unchanged. At a separation distance of 2.5 Å, the charge of the Al–Al bonds is depleted, leading to the ultimate breakage of Al–Al bonds. Meanwhile, the charge densities between Al–Li bonds begin to decay. Nevertheless, these weak bonds are still joined to the interface until the separation displacement reaches 2.6 Å, where no accumulation of the charge density can be observed between these atoms. Eventually, this interfacial structure will split into two individual surfaces.

Figure 7 shows the charge density distributions of the inf-Cu during uniaxial tension. When Cu atoms are initially segregated at the next nearest-neighbor interface, they would enormously increase the charge density here and form strong Cu–Al bonds with the surrounding Al atoms. While they have little effect on the Al–Al and Al–Li bonds at the interface. Looking at change of charge density distributions during the tensile, these strong Al–Al bonds almost fracture at a separation distance of 2.4 Å, which is 0.1 Å shorter than that in the inf-free. Meanwhile, the interface can be still connected via very weak Al–Li bonds until a further displacement of 2.5 Å, in which this interfacial structure is completely fractured. Apparently, Cu atoms segregated at interfacial sites will result in an expansion of the entire interfacial structure. These Cu atoms expand the interplanar spacing of the inf@1 by 0.24 Å, as well as the inf@2 by 0.10 Å. Eventually, the expanded interplanar spacing accelerates the break of

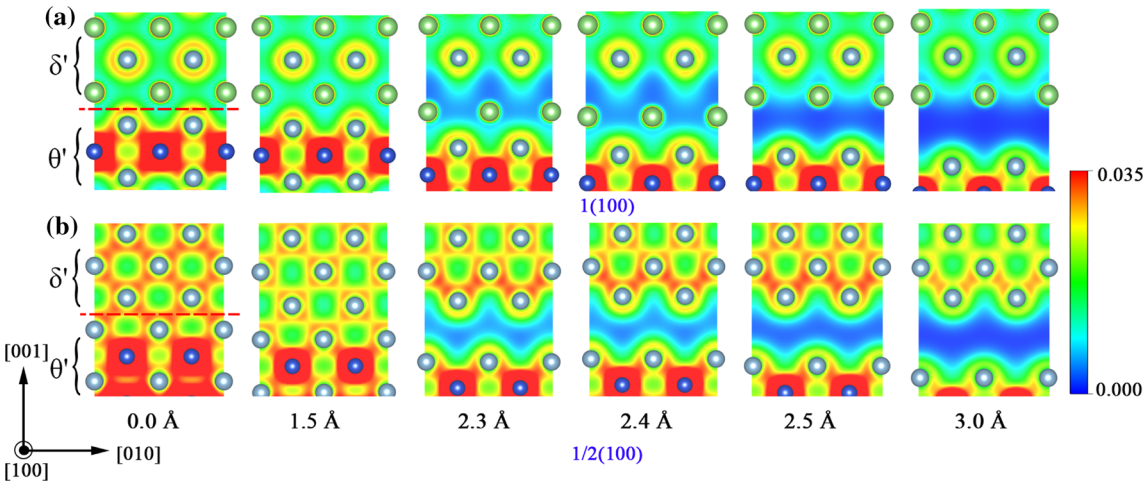

Figure 7 Charge density distributions of the inf-Cu in 1(100) and 1/2(100) planes along with an increased displacement distance (in Å) shown below each frame, using the RGS + relaxation method. The unit is in e/Bohr^3.

the $\delta'/\theta'/\delta'$ along the inf@2. On the other hands, we suggest that these weak Al–Li bonds play an important role in connecting the interface under large tensile displacements. This may be due to the fact that the chemical bonds between Li and Al atoms are relatively weak, and Li atoms can overcome this weak binding during relaxation and connect to the θ' within the maximum migration range.

Conclusion

The thickening and strength of the $\delta'/\theta'/\delta'$ composite precipitate with separations of Cu atoms have been systemically investigated by using first-principle calculations. For the $\delta'/\theta'/\delta'$ composite precipitates with different thicknesses observed in experiments, two thickening models have been proposed under the assumption that the GP-like zone is considered as an intermediate state in the growth process. Combining the evaluation of structures during the growth process with the aging temperature-induced nucleation analysis, we suggest that the thickening mechanism of $\delta'/\theta'/\delta'$ composite precipitate is dependent upon aging temperatures. At elevated aging temperatures, the θ' precipitates can grow rapidly without being covered by δ' phases. On the opposite, δ' phases can precipitate energetically favorably upon the θ', leading to a severe constraint on the growth of the θ'.

After analyzing the methodological flaws of the conventional methodologies, including linear fitting (LF) and direct calculation (DC), for interfacial energy calculations in terms of structure and energy, we proposed a vacuum-added methodology to accurately evaluate the interfacial energy of the complex $\delta'/\theta'/\delta'$. For the inf@2, it possesses a relatively small and negative interfacial energy, suggesting a sharp interface can favorably form here. Interestingly, if the inf@2 is defined as nucleation sites for the δ', which will nucleate spontaneously at relatively low aging temperatures. The $\delta'/\theta'/\delta'$ composite precipitate can basically maintain the total thickness as small as 10 nm and realize the supra-nanostructure. In addition, Cu segregations increase the interfacial energy but reduce the strain energy by coordinating the distortions of two bulk components.

A variety of factors that need to be considered to establish a realistic fracture interface, including the interfacial energy, the final fracture plane after relaxation, and the nucleation order. It is shown that the inf@2 is the most likely fracture interface in the $\delta'/\theta'/\delta'$. Using RGS and RGS + relaxation methodologies, the weakening effects of Cu segregations at the IB have been confirmed, which reduces the theoretical strength by about 20%. The interface expansion caused by Cu segregations leads to strong Al–Al bond breaks, which accelerates the final fracture of the $\delta'/\theta'/\delta'$ composite precipitates along the IB.

Acknowledgements

The authors would like to thank the helps from all lab mates at the Integrated Computational Materials Engineering (ICME) laboratory, Beijing Institute of Technology, China. The funding support from the Key Laboratories at Beijing Institute of Technology (funding#6142902180305, and #61409220124) is greatly acknowledged.

Supplementary Information: The online version contains supplementary material available at https://doi.org/10.1007/s10853-021-05894-2.

References

[1] Dorin T, Vahid A, Lamb J (2018) Chapter 11: aluminium lithium alloys. In: Lumley RN (ed) Fundamentals of aluminium metallurgy. Woodhead Publishing, Cambridge, pp 387–438. https://doi.org/10.1016/B978-0-08-102063-0.00011-4

[2] Jiang B, Wang HS, Yi DQ, Tian Y, Shen FH, Wang B, Liu HQ, Hu Z (2020) Effect of Ag addition on the age hardening and precipitation behavior in an Al–Cu–Li–Mg–Zn–Mn–Zr alloy. Mater Charact 162:110184. https://doi.org/10.1016/j.matchar.2020.110184

[3] Ma PP, Zhan LH, Liu CH, Wang Q, Li H, Liu DB, Hu ZG (2019) Pre-strain-dependent natural ageing and its effect on subsequent artificial ageing of an Al–Cu–Li alloy. J Alloys Compd 790:8–19. https://doi.org/10.1016/j.jallcom.2019.03.072

[4] Kim K, Zhou BC, Wolverton C (2018) First-principles study of crystal structure and stability of T_1 precipitates in Al–Li–Cu alloys. Acta Mater 145:337–346. https://doi.org/10.1016/j.actamat.2017.12.013

[5] Gumbmann E, Lefebvre W, De Geuser F, Sigli C, Deschamps A (2016) The effect of minor solute additions on

the precipitation path of an Al–Cu–Li alloy. Acta Mater 115:104–114. https://doi.org/10.1016/j.actamat.2016.05.050

[6] Miao J, Sutton S, Luo AA (2020) Microstructure and hot deformation behavior of a new aluminium–lithium–copper based AA2070 alloy. Mater Sci Eng A 777:139048. https://doi.org/10.1016/j.msea.2020.139048

[7] Duan SY, Wu CL, Gao Z, Cha LM, Fan TW, Chen JH (2017) Interfacial structure evolution of the growing composite precipitates in Al–Cu–Li alloys. Acta Mater 129:352–360. https://doi.org/10.1016/j.actamat.2017.03.018

[8] Duan SY, Le Z, Chen ZK et al (2016) Li-atoms-induced structure changes of Guinier–Preston–Bagaryatsky zones in AlCuLiMg alloys. Mater Charact 121:207–212. https://doi.org/10.1016/j.matchar.2016.09.037

[9] Yoshimura R, Konno TJ, Abe E, Hiraga K (2003) Transmission electron microscopy study of the early stage of precipitates in aged Al–Li–Cu alloys. Acta Mater 51:2891–2903. https://doi.org/10.1016/s1359-6454(03)00104-6

[10] Wang S, Zhang C, Li X, Huang H, Wang J (2020) First-principle investigation on the interfacial structure evolution of the δ'/θ'/δ' composite precipitates in Al–Cu–Li alloys. J Mater Sci Technol 58:205–214. https://doi.org/10.1016/j.jmst.2020.03.065

[11] Terrones LAH, Monteiro SN (2007) Composite precipitates in a commercial Al–Li–Cu–Mg–Zr alloy. Mater Charact 58:156–161. https://doi.org/10.1016/j.matchar.2006.04.008

[12] Zheng YH, Liu YX, Wilson N et al (2020) Solute segregation induced sandwich structure in Al–Cu(–Au) alloys. Acta Mater 184:17–29. https://doi.org/10.1016/j.actamat.2019.11.011

[13] Bourgeois L, Zhang Y, Zhang Z, Chen Y, Medhekar NV (2020) Transforming solid-state precipitates via excess vacancies. Nat Commum 11(1):1248. https://doi.org/10.1038/s41467-020-15087-1

[14] Bourgeois L, Dwyer C, Weyland M, Nie J-F, Muddle BC (2011) Structure and energetics of the coherent interface between the θ′ precipitate phase and aluminium in Al–Cu. Acta Mater 59:7043–7050. https://doi.org/10.1016/j.actamat.2011.07.059

[15] Griffith AA (1921) The phenomena of rupture and flow in solids. Philos Trans R Soc Lond Ser A Contain Pap Math Phys Character 221:163–198. https://doi.org/10.1098/rsta.1921.0006

[16] Kresse G, Furthmüller J (1996) Efficient iterative schemes for ab initio total-energy calculations using a plane-wave basis set. Phys Rev B 54:11169–11186. https://doi.org/10.1103/PhysRevB.54.11169

[17] Perdew JP, Burke K, Ernzerhof M (1996) Generalized gradient approximation made simple. Phys Rev Lett 77:3865–3868. https://doi.org/10.1103/PhysRevLett.77.3865

[18] Monkhorst HJ, Pack JD (1976) Special points for Brillouin-zone integrations. Phys Rev B 13:5188–5192. https://doi.org/10.1103/PhysRevB.13.5188

[19] Vaithyanathan V, Wolverton C, Chen LQ (2004) Multiscale modeling of θ′ precipitation in Al–Cu binary alloys. Acta Mater 52:2973–2987. https://doi.org/10.1016/j.actamat.2004.03.001

[20] Wang Y, Liu ZK, Chen LQ, Wolverton C (2007) First-principles calculations of β″-Mg_5Si_6/α-Al interfaces. Acta Mater 55:5934–5947. https://doi.org/10.1016/j.actamat.2007.06.045

[21] Butler KT, Gautam GS, Canepa P (2019) Designing interfaces in energy materials applications with first-principles calculations. NPJ Comput Mater 5:19. https://doi.org/10.1038/s41524-019-0160-9

[22] Spowage AC, Bray S (2010) Characterization of nanoprecipitation mechanisms during isochronal aging of a pseudo-binary Al-8.7 at. pct Li alloy. Metall Mater Trans A 42:227–230. https://doi.org/10.1007/s11661-010-0498-6

[23] Neibecker P, Leitner M, Kushaim M, Boll T, Anjum D, Ta A-K, Haider F (2017) $L1_2$ ordering and δ′ precipitation in Al–Cu–Li. Sci Rep 7:3254. https://doi.org/10.1038/s41598-017-03203-z

[24] Okuda H, Tanaka I, Osamura K, Osawa M, Amemiya Y (1997) Simultaneous SAS and 100 experiments on phase decomposition and reversion in Al–Li binary alloys. J AppI Cryst 30:586–591. https://doi.org/10.1107/S0021889897002409

[25] Yoshimura R, Konno TJ, Abe E, Hiraga K (2003) Transmission electron microscopy study of the evolution of precipitates in aged Al–Li–Cu alloys: the θ′ and T_1 phases. Acta Mater 51:4251–4266. https://doi.org/10.1016/s1359-6454(03)00253-2

[26] Biswas A, Siegel DJ, Wolverton C, Seidman DN (2011) Precipitates in Al–Cu alloys revisited: atom-probe tomographic experiments and first-principles calculations of compositional evolution and interfacial segregation. Acta Mater 59:6187–6204. https://doi.org/10.1016/j.actamat.2011.06.036

[27] Hui J, Wang L, Wang B (2020) Theoretical study of the effects of alloying elements on Cu nanotwins. Sci China Phys Mech Astron 63:104612. https://doi.org/10.1007/s11433-020-1543-8

[28] Zhao DD, Li YJ (2018) Carbon segregation at Σ3{1 1 2} grain boundaries in silicon. Comput Mater Sci 143:80–86. https://doi.org/10.1016/j.commatsci.2017.11.001

[29] Tian JZ, Zhao YH, Hou H, Han PD (2017) First-principles investigation of the structural, mechanical and

thermodynamic properties of Al_2Cu phase under various pressure and temperature conditions. Solid State Commun 268:44–50. https://doi.org/10.1016/j.ssc.2017.09.016

[30] Wang Y, Meng Y, Wang J, Zhang C, Huang H (2020) Mechanical properties of defective $L1_2$–Al_3X (X = Sc, Lu) phase: a first-principles study. J Rare Earths 39:217–224. https://doi.org/10.1016/j.jre.2020.04.006

[31] Lazar P, Podloucky R (2008) Cleavage fracture of a crystal: density functional theory calculations based on a model which includes structural relaxations. Phys Rev B 78:10414. https://doi.org/10.1103/PhysRevB.78.104114

[32] Janisch R, Ahmed N, Hartmaier A (2010) Ab initio tensile tests of Al bulk crystals and grain boundaries: universality of mechanical behavior. Phys Rev B 81:184108. https://doi.org/10.1103/PhysRevB.81.184108

[33] Zhao DD, Løvvik OM, Marthinsen K, Li YJ (2018) Segregation of Mg, Cu and their effects on the strength of Al Σ5 (210)[001] symmetrical tilt grain boundary. Acta Mater 145:235–246. https://doi.org/10.1016/j.actamat.2017.12.023

[34] Khachaturyan AG, Lindsey TF, Morris JW (1988) Theoretical investigation of the precipitation of δ' in Al–Li. Metall Mater Trans A 19:249–258. https://doi.org/10.1007/BF02652533